ACS APPLIED MATERIALS & INTERFACES

Research Article

www.acsami.org

Synthesis and Phase Evolutions in Layered Structure of Ga_2S_3 Semiconductor Thin Films on Epiready GaAs (111) Substrates

H. F. Liu,* K. K. Ansah Antwi, N. L. Yakovlev, H. R. Tan, L. T. Ong, S. J. Chua, and D. Z. Chi

Institute of Materials Research and Engineering (IMRE), A*STAR (Agency for Science, Technology and Research), 3 Research Link, Singapore 117602, Singapore

Supporting Information

ABSTRACT: We report on synthesis and properties of p-type Ga_2S_3 semiconductor thin films that were prepared by sulfurizing epiready n-type GaAs (111) surface at elevated temperatures. Comparisons of structural and optical properties among the thin films, peeling-off resulted microtubes, and the remains after peeling-off give a clear clue to the crystal growth and phase evolutions of Ga_2S_3. Three layers of Ga_2S_3 are clearly identified in the thin films. They are layer i, cubic Ga_2S_3 epitaxially grown on the GaAs (111) substrate; layer ii, polycrystalline cubic Ga_2S_3 on top of layer-i; and layer iii, monoclinic and/or hexagonal Ga_2S_3 on top of layer ii. The onset of peeling-off occurred in layer i and/or at the interface between layer i and ii. Both the phase evolutions and the location of peeling-off are associated with a Ga out diffusion growth mechanism. Absorption spectroscopy revealed a direct bandgap of 3.0 eV, whereas photoluminescence spectra showed defects (excited Ga vacancies) related red (1.62 eV) and green (2.24 eV) emissions of the Ga_2S_3 films; both are qualitatively consistent with those reported values obtained at lower sample temperatures from Ga_2S_3 single crystals. These results, together with a large on/off current ratio (i.e., ~14 at a bias of 4.0 V) of the resultant hetero p-Ga_2S_3/n-GaAs junction under a blue laser (405 nm, 3.0 mW) illumination, shed light on consequent integrations of Ga_2S_3- and GaAs-based optoelectronic devices, e.g., high-power laser radiation sensors.

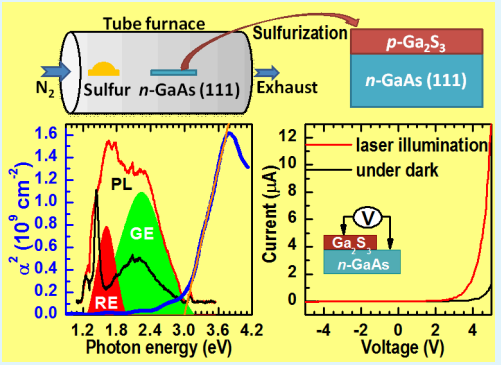

KEYWORDS: *Ga_2S_3, sulfurization, phase change, atom diffusions, photoluminescence, laser-radiation sensing*

1. INTRODUCTION

Ga_2S_3, a representative of $A_2^{III}B_3^{VI}$ compounds, has long been studied as an imperfect semiconductor that has 1/3 unoccupied vacancies in its Ga sublattice.[1,2] Recent studies revealed that Ga_2S_3 has not only a very high laser-induced damage threshold (LIDT) but also a large second-harmonic generation efficiency; both factors are desired for nonlinear optical applications.[3] From the application point of view, studies reported in the literature on Ga_2S_3 can be generally cataloged into two groups. One is focused on synthesis, doping controlling, and material characteristics for optical and optoelectronic applications, e.g., light-emitting diodes (LED) and UV-absorber in photovoltaic devices, because of its direct and wide band-gap of ~3.4 eV.[2−6] The other is more focused on surface passivation of III−V semiconductors, i.e., to form a "native" sulfide layer on GaAs or InP via surface sulfurizations; so that the surface recombination of GaAs or InP can be dramatically suppressed, which in turn significantly improves the device performances.[7,8] The former group is usually dealing with "bulk" Ga_2S_3 crystals, whereas the latter one is mainly handling ultrathin Ga_2S_3 layers (thinner than a few nanometers) on hetero-structural surfaces. In contrast, the formation of 'thick' Ga_2S_3 layers on a hetero-substrate (e.g., GaAs) and the thickness increment induced interfacial properties, which are interesting and desired in the field of materials science and engineering, are lacking in the literature.[3,9] Moreover, Ga_2S_3/GaAs heterostructures and their growth technology can have important consequence in fabricating novel Ga_2S_3−GaAs integrated optical and optoelectronic devices.

In this work, we attempt to shed some light on preparing "thick" Ga_2S_3 films (~500 nm) on n-type GaAs (111) substrate via thermal vapor sulfurization at elevated temperatures in a tube-furnace system.[10] The structural and optical properties of so-obtained Ga_2S_3 layers have been systematically studied by using various techniques. They revealed an apparent cubic-to-monoclinic/hexagonal phase change in the crystal structure of the Ga_2S_3 layer along the film growth direction. They also revealed a direct bandgap of 3.0 eV and dual defect-related emissions at room temperature; both are qualitatively consistent with those observed at lower sample temperatures from bulk Ga_2S_3 single crystals. The resultant Ga_2S_3/GaAs heterostructure, when simply fabricated into a mesa-diode, exhibits a typical current rectifying characteristic. The thermal vapor sulfurization method could also be helpful in fabricating GaS layers that have been demonstrated by Barron et al. to be

Received: December 9, 2013
Accepted: January 7, 2014
Published: January 7, 2014

   dx.doi.org/10.1021/am4056535 | ACS Appl. Mater. Interfaces 2014, 6, 3501−3507

effective surface passivation layers for GaAs as well as gate insulators for GaAs transistors.[11,12]

2. EXPERIMENTAL PROCEDURE

2.1. Thermal Sulfurization of Ga_2S_3 Layered Structures. The tube-furnace system employed for the thermal vapor sulfurization of GaAs is the same as the one used for growing MoS_2 two-dimensional materials reported in ref 10. The 2 in. diameter epiready Si-doped n-type GaAs (111) substrates used in this study, 350 ± 10 μm in thickness, were purchased from Wafer Technology Ltd. UK. After loading the substrate into the tube-furnace chamber, the chamber was purged with flowing nitrogen, which was also used as the carrier gas during sulfurization, for 2 h. The thermal sulfurization was started by increasing the furnace temperature to 450 °C within 20 min and then to 650 °C in another 20 min. After keeping the temperature at 650 °C for 20 min, the heating power was turned off and furnace was naturally cooled to room temperature. The continuous supply of sulfur vapor throughout the entire sulfurization process was realized by using two separated source crucibles, located in the up-stream of the flowing nitrogen at different distances from the GaAs substrate.

2.2. Characterizations. After sulfurization, structural and optical properties were characterized, focusing on samples from adjacent areas of the 2-inch wafer: (i) where the film peeling-off occurred, named exposed area (EA); (ii) where there is no film peeling-off, named film-on-substrate (FOS); and (iii) the free-standing (FS) microtubes that were formed because of film peeling-off and rolling-up. For these characterizations we have employed x-ray diffractometer (XRD, Bruker-D8) equipped with a general-area detector that has the advantage of being highly sensitive to crystal phase structures. X-ray florescence (XRF, Bruker M4 TORNADO) was employed to analyze the chemical compositions of the peeled-off films, in which the effect of the GaAs substrate is completely eliminated. Secondary ion-mass spectroscopy (SIMS) was performed in a time-of-flight mass spectrometer (ION-TOF GmbH). Cs (3 kV, 14 nA) and Bi (25 kV, 0.6 pA) were used as the sputtering and analysis beams, respectively. Negative secondary ions were collected not only for the intrinsic elements (i.e., S, Ar, Ga) but also for contaminate elements (e.g., C, O, Cl, etc.). Field-emission scanning-electron microscopy (SEM, Joel JSM-6700F) and transmission-electron microscopy (TEM, Philips CM300 FEGREM) equipped with energy-dispersive x-ray spectrometer (EDX) were employed for imaging and chemical analysis of the samples. Micro-Raman measurements were carried out using both 514 and 325 nm laser lines as the excitation sources, whereas the photoluminescence (PL) spectra were collected using a 405 nm laser as the excitation source. Both the Raman and the PL measurements were carried out at room temperature under microscopes in a backscattering or surface normal reflection configuration.

3. RESULTS AND DISCUSSION

3.1. Sulfurized Thin Films and Chemical Analysis. Figure 1a shows an image taken under a nomarski microscope from adjacent areas, so named EA and FOS, of the sulfurized wafer. Likewise, shown in Figure 1b is an image of a typical FS microtube that was peeled-off from the area corresponding to that of EA. The clue of rolling-up and overlapping is clearly seen in Figure 1b from the middle to the left. The image shown in the inset of Figure 1c is recorded by an in situ camera of the XRF chamber and the small circle indicates the location of the XRF analysis on the FS microtube. One can clearly see that the XRF spectrum in Figure 1c exhibits solely S and Ga elements along with those of Zr, Rh (caused by the x-ray tube and detector) and Ar (due to the air environment); there is no As detectable at all. A careful analysis of the XRF spectrum revealed that the Ga-to-S atom ratio is about 1:1.5, implying that the FS sample is most likely of Ga_2S_3 compound because the effect of the GaAs substrate on the XRF measurement is completely eliminated from the FS sample.

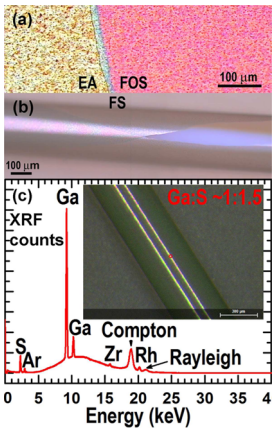

Figure 1. (a) Surface image recorded by Nomarski microscope from adjacent areas of exposed area (EA) and film-on-substrate (FOS); (b) image recorded by Nomarski microscope from a free-standing (FS) microtube formed due to film peeling-off and rolling-up; (c) XRF spectrum collected from a FS microtube. The image in c is recorded by an in situ camera showing the location of XRF analysis.

However, Ga_2S_3 has long been demonstrated to have different crystal phases, including monoclinic, hexagonal, and cubic.[6] Phase identification between monoclinic and hexagonal is quite a challenge for Ga_2S_3 layered structures, where most of the XRD peaks appear at the same angles S1 (Supporting Information). This is because there is only a small distortion in the lattice structures between monoclinic and hexagonal Ga_2S_3. Figure 2a–c shows the XRD scans collected from the FS, FOS,

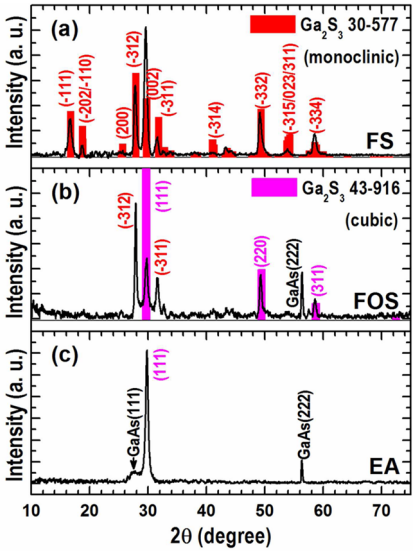

Figure 2. XRD scans collected from (a) the free-standing (FS) microtubes, (b) the film-on-substrate (FOS) structure, and (c) the exposed area (EA) where film was peeled-off. The columnar patterns in a and b are the ICDD-PDFs of monoclinic and cubic Ga_2S_3, respectively.

and EA samples, respectively. The ICDD-PDFs of monoclinic Ga_2S_3 (30-577) and cubic Ga_2S_3 (43-916) are shown together with the spectra in panels a and b in Figure 2, respectively. One can see that they are matching the XRD scans very well; however, because of the difficulty in phase identification between monoclinic and hexagonal Ga_2S_3 and for the sake of brevity, hereafter, we would assign the structure in FS mainly to

dx.doi.org/10.1021/am4056535 | ACS Appl. Mater. Interfaces 2014, 6, 3501–3507

monoclinic Ga_2S_3 (Figure 1a); but it is not necessarily meaning the absence of hexagonal Ga_2S_3 because they have only a small distortion in the crystal lattice from one to another.

3.2. Layered Structures of Sulfurized Ga_2S_3. A careful comparison in Figure 2a reveals that the XRD peak at about 30° is much larger in intensity than that of the ICDD-PDF pattern, whereas in Figure 2b, both (−312) and (−311) of monoclinic Ga_2S_3 appear along with cubic Ga_2S_3. It has to be noted that the cubic Ga_2S_3 (111) peak in Figure 2b is intentionally suppressed to save the detector during the XRD measurement. A comparison between panels a and b in Figure 2 provides evidence that cubic Ga_2S_3 is also incorporated in the FS sample, whereas the phase incorporation of monoclinic Ga_2S_3 in FOS is largely reduced as compared to that in FS; the latter case is also confirmed by the absence of the typical peaks of monoclinic Ga_2S_3 (−111) and (−202/−110) (i.e., those at 16−20° in Figure 2b). The XRD spectrum in Figure 2c exhibits a single peak at about 30° along with those of GaAs (111) and (222); here, again, the GaAs (111) is intentionally suppressed to save the detector. In connection with panels a and b in Figure 2, the single peak in Figure 2c can be assigned to cubic Ga_2S_3 (111). This assignment, in turn, indicates that the remained cubic Ga_2S_3 layer in the EA sample has a preferred growth orientation of Ga_2S_3 (111)//GaAs (111). A further cross-sectional TEM observation revealed that the cubic Ga_2S_3 in layer-i was epitaxially grown on GaAs S2 (see the Supporting Information).

Based on these observations, we can identify that three layers of Ga_2S_3 have been formed in sequent, stacking on the GaAs (111) substrate. They are layer i, epitaxial cubic Ga_2S_3 (at the bottom); layer ii, polycrystalline cubic Ga_2S_3 (in the middle); and layer iii, polycrystalline monoclinic Ga_2S_3 (at the top). The peeling-off of the Ga_2S_3 film occurred in layer i and/or at the interface between layer i and layer ii. Phase change from cubic to monoclinic Ga_2S_3 also occurred in layer ii during the peeling-off and rolling-up, which resulted in the significantly increased phase compositional ratio of monoclinic-to-cubic in the FS sample (Figure 2a) as compared with that in the FOS sample (Figure 2b). This phenomenon, i.e., phase change from epitaxially grown cubic Ga_2S_3 in layer i through the polycrystalline cubic Ga_2S_3 in layer ii to the polycrystalline monoclinic Ga_2S_3 in layer iii, as well as the Ga_2S_3 phase change from cubic to monoclinic induced by peeling-off and rolling-up, could be due to the same mechanism as that reported by Tomas et al.,[6] where the phase change of Ga_2S_3 from hexagonal to monoclinic induced by electron-beam heating during the TEM observations was attributed to a cation diffusion process.

It is well-known that during S adsorption on GaAs at elevated temperatures, the surface of GaAs loses As gradually, being replaced by S, while Ga remains intact, so that a close-packed two-dimensional Ga_2S_3 layer is formed on GaAs.[8] In this case, the Ga_2S_3 layer is most likely resulted in the same cubic crystal structure of the GaAs substrate. However, the large lattice mismatch between Ga_2S_3 and GaAs tends to induce large lattice strain in the sulfide layer, which disrupts the overlayers thicker than a few monolayers. This, in turn, contributes to the phase changes of Ga_2S_3 at elevated temperatures. Because the growth mechanism of Ga_2S_3 thicker than a few nanometers on GaAs, especially by thermal vapor sulfurization, is lacking in the literature, which is next addressed by carrying out SIMS and TEM studies of the resultant Ga_2S_3 layered structures.

3.3. Ga_2S_3 Growth Mechanism and Film Peeling-off. Panels a and b in Figure 3 present the SIMS spectra of Ga−As,

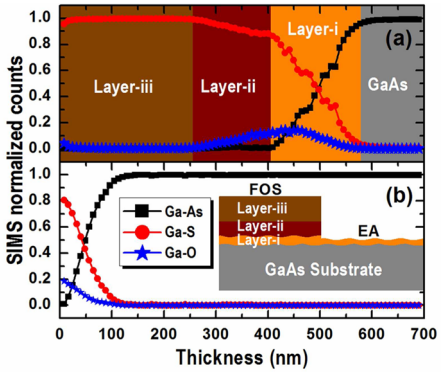

Figure 3. SIMS spectra collected from (a) the film-on-substrate (FOS) area and (b) the exposed area (EA). The inset in b shows the schematic cross-section structure of the Ga_2S_3/GaAs layered structure as well as the most possible peeling-off location.

Ga−S, and Ga−O ions collected from the FOS and EA samples, respectively (see the schematic in Figure 3b). The thickness was calibrated in terms of the cross-sectional TEM images S2 (see the Supporting Information). The three-layer-structure identified by XRD on GaAs is clearly seen and indicated in Figure 3a. A comparison between panels a and b in Figure 3 provides clear-cut evidence that the film peeling-off occurred in layer i or at the interface between layer i and layer ii. The most important observation in Figure 3a is that O present in layer i and layer ii rather than in layer iii. In fact, other contaminations such as C and Cl exhibit the same depth profiles as that of O, whereas As is significantly reduced and negligible in layer ii and iii S3 (see the Supporting Information), which is consistent with the XRF result in Figure 1c. The distribution of contaminate elements is a native "interface marker,"[13] indicating the original surface location of the starting GaAs substrate. The existence of O in layer i and ii but not in layer iii, together with the absence of As in layer ii and iii, thus indicates that the continuous growth of Ga_2S_3 was realized via reactions of S and Ga on the surface of the sulfide layer; the Ga atoms were supplied via out diffusions from the GaAs substrate, through the grown sulfide layer, onto the growing surface. This sulfide growth mechanism is in contrast to the formation of In_2O_3/InN and GeS/GeS_2 multilayers, which involve solely O and S inward diffusions through the oxide and sulfide layers, respectively.[13−15] This mechanism is also in contrast to metal (e.g., Fe) sulfurizations,[16] where both S atoms inward diffuse (through the FeS_2 layer on top) and Fe atoms outward diffusion (through the FeS layer at the bottom) occur. The solely out diffusion of Ga atoms, through the grown Ga_2S_3 layer, onto the growing surface has not been reported in the literature. However, this mechanism is physically reasonable because the Ga sublattice of Ga_2S_3 is 1/3 unoccupied (i.e., occupied by lattice vacancies),[6,17,18] which is feasible for Ga atom diffusions at elevated temperatures. On the other hand, the intermediate Ga_2S_3 layer has the same crystal structure as that of the GaAs substrate, which tends to suppress the formation of non-stoichiometric monosulfide other than those in Fe sulfurizations.[16] The out diffusion of Ga in the grown Ga_2S_3, together with the building-up strain, thus resulted in the phase changes in layer ii and iii, supporting the phase change mechanism proposed by Tomas et al.[6] as discussed above.

dx.doi.org/10.1021/am4056535 | ACS Appl. Mater. Interfaces 2014, 6, 3501−3507

Because neither XRF nor SIMS can detect the presence of As in layer iii and ii, we believe that As was evaporated from the GaAs surface in the initial sulfurization stage. However, the increase in the thickness of the grown sulfide layer tends to block the surface evaporation of As. Instead, As was turned to diffusion deeper into the GaAs substrate (much thicker than the surface and interface layers) at elevated temperature. The backward diffusion of As atoms in the GaAs substrate may introduce some point defects, e.g., As antisite (As_{Ga}), As interstitials (As_i), complex formed by Ga vacancy (V_{Ga}) and As_i, etc.[19,20] This is in fact supported by the observation that a gap-state PL emission from the GaAs substrate of a FOS sample is significantly enhanced when a longer wavelength laser excitation is employed in the PL measurement (to be discussed later).

Presented in Figure 4a is a top-view SEM image recorded from FOS and EA in adjacent areas on the 2 in. wafer. Onset of

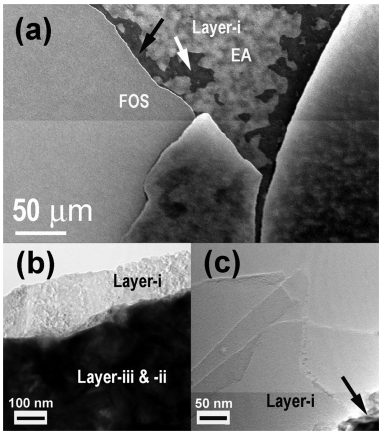

Figure 4. (a) SEM image recorded from the adjacent areas of an exposed area (EA) and a film-on-substrate (FOS) area, the arrows indicate the typical locations near the boundary where layer i was partly peeled-off together with layers on top. (b, c) TEM images showing the peeled-off layers. The parts of layer i in b and c correspond to those areas indicated by arrows in a, whereas the arrow in c indicates the layers with larger thickness on top of layer i.

fragmental peeling-off with layer i left behind is seen in the lower middle part. However, some pieces of layer i, e.g., those indicated by arrows in Figure 4a, were peeled-off together with layer ii and iii, which is further evidenced in the top-view TEM images b and c shown in Figure 4 recorded from the FS samples. Here, the TEM specimens were prepared by fishing the acetone-dissolved FS fragments using Cu grids covered by amorphous carbon films. It is clearly seen in images b and c in Figure 4 that layer i (very thin in thickness, showing bright contrast) extended out the edge of layer iii and ii (indicated by the arrow in Figure 4c). A combination of image a and images b and c in Figure 4 provides clear evidence that the film peeling-off occurred in layer i and/or at the interface between layer i and layer ii (see Figure 3), supporting the XRD results. The reason that the film peeling-off occurred in layer i might be related to the solely Ga diffusion growth mechanism of Ga_2S_3. It is well-known that in lattice mismatched hetero-epitaxy, strain builds up with the increase in epilayer thickness. The largest lattice strain generally distributes at the initial hetero-interface, leading to the generation of dislocations therein. In case of Ga_2S_3/GaAs heterostructure both the thickness increment of Ga_2S_3 and the out diffusion of Ga atoms can generate a defective region at the Ga_2S_3/GaAs interface or in layer i. Moreover, mismatch in thermal expansion coefficients of Ga_2S_3 and GaAs may also contribute to the peeling-off at the defective Ga_2S_3/GaAs interface during the sample cooling down from the growth temperature. It is worth mentioning that the Ga-to-S atomic ratios measured by the micro-scale EDX from the TEM specimens at various locations are about 1:1.5 S4 (see the Supporting Information), which is consistent with the macroscale XRF result. Meanwhile, there is no As signal detectable at all in the EXD spectra, supporting the XRD and SIMS results.

3.4. Phonon Softening and Strain Redistribution. Figure 5 shows the Raman scattering spectra collected from

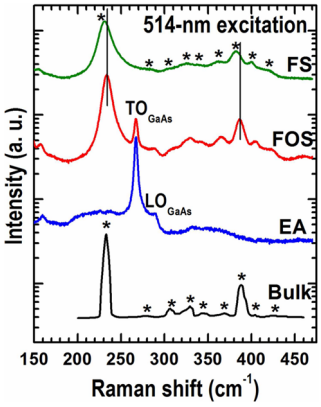

Figure 5. Raman spectra collected at room temperature using a 514 nm laser as the excitation light source. A Raman spectrum of a bulk Ga_2S_3 single crystal is also displayed for comparisons.

the Ga_2S_3 samples of FS, FOS, and EA. For easier comparisons, a Raman scattering spectrum of a bulk Ga_2S_3 single crystal is also presented. It has to be noted that because of the small distortion in the lattice structures of Ga_2S_3 polymorphisms the differences in Raman spectra of monoclinic and hexagonal Ga_2S_3 are too small to be distinguished.[21] It is seen in Figure 5 that the spectrum of the FS sample exhibits exactly the same Raman features as those of the bulk Ga_2S_3 single crystal (indicated by asterisks) while the FOS sample, when compared to FS, shows only the extra TO_{GaAs} and LO_{GaAs} modes that originate from the GaAs substrate. These observations confirm that the resultant film consists of Ga_2S_3 crystals. In contrast to FS and FOS, the spectrum of EA is dominant by the TO_{GaAs} and LO_{GaAs} modes of GaAs, even when it is excited by a 325 nm laser S5 (see the Supporting Information). The absence of Ga_2S_3-related Raman features in the spectrum of EA, combined with the facts that layer-i partially remained in EA (see Figures 2c, 3b, and 4a), indicates that the remained layer i is very thin. It is, in fact, about 30−50 nm as seen from the cross-sectional TEM images S2 (see the Supporting Information).

Also seen in Figure 5 is that the Raman features softened in the FS sample as compared to those in the FOS sample. For example, the A_1 mode of the FOS sample locates at 233.87 cm^{-1}, whereas that of the FS sample shifted down to 231.14 cm^{-1}. In general, the softening in phonon vibrational modes manifests itself as either a release of compressive strain or an increase of tensile strain in the Ga_2S_3 layer after peeling-off. A high-resolution XRD scan S6 (see the Supporting Information), using the GaAs (111) diffraction peak as the calibration standard, revealed that the remained layer i is tensile stressed on the GaAs substrate. This is reasonable since cubic Ga_2S_3,

which is the initial layer epitaxially grown on GaAs at the Ga_2S_3/GaAs interface, has a smaller lattice constant (0.522 nm) than that of GaAs (0.565 nm). With this strain verification, it is clear that the phonon softening of Ga_2S_3 after peeling-off is caused by an increase in tensile strain, which could be attributed to strain redistribution in layer ii and iii during the film peeling-off and rolling-up. This is the same as those of strain redistribution in GaN-on-Si multilayer structures caused by wafer curving when the substrate is thinned to a certain thickness (e.g., 4.0 μm in ref 22). In the current case, the tensile strain is larger in layer ii, i.e., the region closer to the GaAs substrate, than in layer iii. During the film peeling-off, layer ii shrinks more than layer iii does to relax the tensile stress, which results in the concaving and rolling of the film into microtubes S7 (see the Supporting Information). The surface concaving and rolling of the peeled-off film thus redistribute the tensile stress into layer iii, i.e., the out surface of the microtube, and thus lead to the photon softening.

3.5. Optical Properties and Photovoltaic Devices. Presented in Figure 6 are the PL spectra collected from the EA and FS samples as well as the optical absorption spectrum (obtained by measuring the transmittance and reflectance, see ref 23) collected from the FS sample; both the PL and the absorption spectra were collected under microscope at room temperature. The PL spectrum of the FOS sample is the same in lineshape as that of FS (thus not shown for the sake of brevity) because of the limited penetration depth of the 405 nm laser in Ga_2S_3. The layer thickness estimated from the optical interference fringes employing the optical parameters reported by Zhang et al.[3] is about 450 nm, consistent with that observed in the cross-sectional TEM images S2 (see the Supporting Information). The linear fitting to the absorption edge in Fig. 6 revealed a direct bandgap of 3.0 eV for the resultant free-standing Ga_2S_3, which falls well in the range of 2.8−3.4 eV reported in the literature.[3,5,24,25] It is obvious that the PL emissions from the FS and EA samples, except for the sharp peak (at 1.43 eV) from the GaAs substrate because of the remaining Ga_2S_3 layer in EA is very thin (see above discussion), are due to defect levels located in the bandgap of Ga_2S_3. The PL spectrum of the FS sample exhibits a broadband emission that can be well deconveluted into a red emission (RE) at 1.62 eV and a green emission (GE) at 2.24 eV by using Lorentzian-function fittings, which are shown together with the PL spectra in Figure 6. If the effect of sample temperature is taken into account, one can see that these two emission peak energies are rather consistent with those (i.e., at 1.75 and 2.38 eV, respectively) observed by Aono and Kase from Ga_2S_3 single crystals at a lower sample temperature (97 K).[26,27] Furthermore, taking the bandgap of 3.0 eV of the studied Ga_2S_3 into account, the green emission can be readily assigned to electron transitions from conduction-band minimum (CBM) and/or shallow-donor (SD) levels to excited Ga vacancies (~0.7 eV above the valence band).[24,26] Likewise, the red emission can be attributed to electron transitions from a deeper-donor (DD) level to the excited Ga vacancies S8 (see the Supporting Information).[5,24,26]

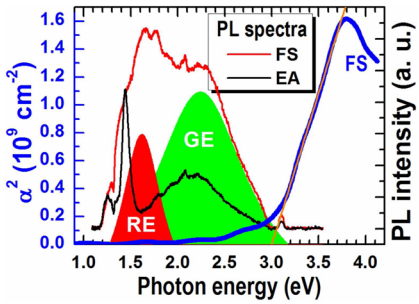

Figure 6. PL and absorption spectra collected at room temperature from the free-standing (FS) and exposed area (EA) samples. A 405 nm laser was used in the PL measurements. The shadowed emission peaks are the best Lorentzian function fittings to the PL spectrum of the FS sample; the straight line in the absorption spectrum is a linear fitting to the absorption edge.

It is worth mentioning that another PL system equipped with a 532 nm Nd:YAG laser and a 325-nm He−Cd laser has also been used for the PL measurements at room temperature. However, this PL system is not suitable for handling the FS samples and the measurements were only carried out on a FOS sample S9 (Supporting Information). It is found that the PL spectrum of the FOS sample yielded by the 325-nm laser excitation is similar, in both the lineshape and the peak positions, to that of the FS sample yielded by the 405-nm laser excitation (see Figure 6). This is quite reasonable because the 325 nm laser, in terms of the absorption spectrum in Figure 6, has a short penetration depth in the Ga_2S_3 overlayer and thus the GaAs substrate is not excitable. On the other hand, when the 532 nm laser excitation is employed, the PL emission of Ga_2S_3 nearly completely disappeared. This is because the excitation energy (i.e., 2.33 eV) is smaller than the bandgap of Ga_2S_3 (i.e., 3.0 eV). As a result, the excitation is ineffective in the Ga_2S_3 overlayer. However, because of the lower absorption of the 532 nm laser in the Ga_2S_3 overlayer, the excitation in the GaAs substrate is more effective, which led to a well-developed PL emission peak at the lower energy side of the GaAs PL emission (1.43 eV) S9 (see the Supporting Information). This gap-state PL emission from the GaAs substrate is readily related to point defects, e.g., As_{Ga}, As_i, V_{Ga}-As_i complex, etc.,[19,20] that were introduced by the backward diffusion of As atoms during the sulfurization at elevated temperature.

A careful comparison between the PL spectra from FS and EA revealed that the RE emission has been vanished from the EA sample (see Figure 6), which could be related to the effect of GaAs below layer-i in EA. It is well known that an ultrathin Ga_2S_3 layer can effectively form a passivation on the GaAs surface via replacing As by S atoms. Vice versa, this passivation behavior can also affect the surface/interface defect states of Ga_2S_3, typically for such a very thin layer. The bandgap energy of Ga_2S_3 is much larger than that of GaAs, in principle, its conjunction with GaAs tends to have increased influences on the DD levels than on the SD ones, leading to the annihilation of RE, whereas a reduced intensity in GE. Nevertheless, more work is needed to verify the detailed annihilation mechanism of the defect-related PL emissions of Ga_2S_3.

Finally, a two-terminal device, schematically shown in the inset of Figure 7, was simply fabricated using the resultant Ga_2S_3/GaAs heterostructure, which has a 3 × 3 mm^2 Ga_2S_3 mesa defined on the n-type GaAs substrate. Presented in Figure 7 are the current−voltage profiles measured from the two-terminal device with and without laser illuminations. Three lasers with different wavelengths, i.e., red (650 nm), green (532 nm), and blue (405 nm), were employed as the light source (i.e., illuminating the Ga_2S_3 mesa) for the device test; the laser powers were adjusted to about 3.0 mW. The photon energy of the former two is smaller than that of the latter one, which is

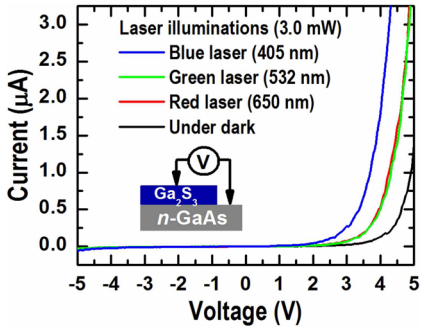

Figure 7. Current–voltage rectifying characteristics of the p-Ga_2S_3/n-GaAs heterojunction under laser illustrations. The laser power on the Ga_2S_3 mesa is about 3.0 mW.

nearly the same as the bandgap energy of the Ga_2S_3 layer (see the absorption spectrum in Figure 6). It is clearly seen in Figure 7 that the profiles exhibit a typical current rectifying characteristic as those diodes. To confirm that the current rectifying characteristic is from the Ga_2S_3/GaAs heterojunction rather than the metal–semiconductor contacts, we have collected the current–voltage profiles from the Ga_2S_3 layer and GaAs substrate, respectively; both of them exhibit ohmic contact behavior S10 (see the Supporting Information). These results thus indicate that the mesa-diode performance is due to the p-Ga_2S_3/n-GaAs heterojunction. The p-type electrical conductive property of the resultant Ga_2S_3 layer is readily attributed to the presence of Ga vacancies, which are generally acceptors in Ga_2S_3 (see S8 in the Supporting Information)[24,26] It is also seen that laser illustrations, especially the blue one, significantly enhanced the current at the biases larger than 1.0 V. The similar current enhancement effect of the red and green lasers is mainly due to the contribution from the n-GaAs since the absorption coefficient of the red and green light in Ga_2S_3 is very small. In contrast, the larger current enhancement effect of the blue laser is mainly contributed by the p-type Ga_2S_3 due to its increased absorption coefficient (see Figure 6). The on/off current ratio at a bias of 4.0 V, when employing the blue laser illustration, is about 14. This result, together with the reported high LIDT of Ga_2S_3,[3] suggests that the p-Ga_2S_3/n-GaAs mesa-diode has a great potential in high-power laser sensing applications.

4. CONCLUSIONS

In conclusion, p-type Ga_2S_3 layered structures of about 500 nm in thickness have been prepared on epiready n-type GaAs (111) substrate by thermal vapor sulfurization at elevated temperatures. The growth of Ga_2S_3 is realized by Ga atoms out-diffusion from the GaAs substrate, through the grown sulfide layer, onto the growing surface. The Ga atoms diffusion process, together with the building strain in the Ga_2S_3 layer, leads to its phase change from epitaxial cubic to polycrystalline monoclinic and/or hexagonal polymorphisms along the growth direction, as well as to the film peeling-off at and/or close to the Ga_2S_3/GaAs interface. As atoms are evaporated from the GaAs surface in the initial sulfurization stage, however, an increase in the thickness of the grown sulfide tends to block the As surface evaporations. Instead, we believe that As was turned to diffuse deeper into the GaAs substrate, which is much thicker than the surface layers. This conclusion is drawn based on the fact that As could be detected neither in the peeled-off films nor in the near-surface area of the Ga_2S_3/GaAs heterostructure. A direct bandgap of 3.0 eV is revealed for so-obtained Ga_2S_3 thin films, which falls well in the range of 2.8–3.4 eV reported in the literature. Defect-related red and green emissions at 1.62 and 2.24 eV, respectively, have been observed at room temperature from the Ga_2S_3 films; both of them, especially the red emission, are sensitive and weakened by the conjunction with GaAs. We have also demonstrated that the resultant p-Ga_2S_3/n-GaAs heterostructures have a great potential in sensor applications for high-power lasers.

■ ASSOCIATED CONTENT

Supporting Information

XRD patterns of Ga_2S_3 (Figure S1), cross-sectional TEM and SAED images (Figure S2), SIMS depth profiles (Figure S3), an EDX spectrum collected from the TEM specimen in the TEM chamber (Figure S4), UV-Raman spectra (Figure S5), a HRXRD pattern (Figure S6), a top-view SEM image (Figure S7), optical transition diagram (Figure S8), PL spectra (Figure S9), and current–voltage profiles (Figure S10). This material is available free of charge via the Internet at http://pubs.acs.org.

■ AUTHOR INFORMATION

Corresponding Author

*E-mail: liuhf@imre.a-star.edu.sg. Phone: (+65)-68748047. Fax: (+65)-68747744.

Notes

The authors declare no competing financial interest.

■ ACKNOWLEDGMENTS

The authors thank P. C. Lim for collecting the XRD and XRF spectra. S. Tripathy and S. B. Dolmanan are acknowledged for their help in Raman scattering.

■ REFERENCES

(1) Srivastava, P.; Sharma, Y. *AIP Conf. Proc.* **2011**, *1391*, 495–497.
(2) Paorichi, C.; Zuccalli, G. *J. Cryst. Growth* **1970**, *7*, 265–266.
(3) Zhang, M.; Jiang, X.; Zhou, L.; Guo, G. *J. Mater. Chem. C* **2013**, *1*, 4754–4760.
(4) Shaikh, H. A. Ei.; Abdal-Rahman, M.; Belal, A. E.; Ashraf, I. M. *J. Phys. D: Appl. Phys.* **1996**, *29*, 466–469.
(5) Yoon, C.; Medina, F. D.; Martinez, L.; Park, T.; Jin, M.; Kim, W. *Appl. Phys. Lett.* **2003**, *83*, 1947–1949.
(6) Tomas, A.; Guymont, M.; Pardo, M. P.; Guittard, M.; Flahaut, J. *Phys. Status Solidi (a)* **1988**, *107*, 775–784.
(7) Chiu, H.; Huang, Y.; Chang, L.; Chien, F. *Semicond. Sci. Technol.* **2008**, *23*, 035029–5.
(8) Barbouth, N.; Berthier, Y.; Oudar, J.; Moison, J. -M.; Bensoussan, M. *J. Electrochem. Soc.: Solid-State Sci. Technol.* **1986**, 1663–1666.
(9) D. Smyth-Boyle, K. Govender, P. Hazelton, P. O'Brien, Low temperature solution deposition of gallium sulfide thin films for photovoltaic applications. In *Proceedings of the 203rd Meeting of the Electrochemical Society*; Paris, April 28–30, 2003 ; The Electrochemical Society: Pennington, NJ, 2003.
(10) Liu, H. F.; Ansah Antwi, K. K.; Chua, S. J.; Chi, D. Z. *Nanoscale* **2014**, *6*, 624–629.
(11) Tabib-Azar, M.; Kang, S.; Maclnnes, A. N.; Power, M. B.; Barron, A. R.; Jenkins, P. P.; Hepp, A. F. *Appl. Phys. Lett.* **1993**, *63*, 625–627.
(12) Jenkins, P. P.; Maclnnes, A. N.; Tabib-Azar, M.; Barron, A. R. *Science* **1994**, *263*, 1751–1753.
(13) Liu, H. F.; Yakovlev, N. L.; Chi, D. Z.; Liu, W. Post-growth thermal oxidation of wurtzite InN thin films into body-center cubic In2O3 for chemical/gas sensing applications. *J. Solid State Chem.* [Online early access]. Published Online: Oct 18, 2013. http://dx.doi.org/10.1016/j.jssc.2013.10.017 (accessed Oct 18, **2013**).

(14) Liu, H. F.; Chi, D. Z.; Liu, W. *CrystEngComm* **2012**, *14*, 7140−7144.
(15) Repinsky, S. M.; Semyonova, O. I. *Thin Solid Films* **1981**, *75*, 391−403.
(16) Pimenta, G.; Kautek, W. *Thin Solid Films* **1992**, *219*, 37−45.
(17) Askerov, I. M.; Mekhrabov, A. O.; Aslanov, C. K.; Tagiev, B. G.; Nakhmetov, S. M. *Phys. Stat. Sol. (a)* **1988**, *105*, K151−K154.
(18) Guymont, M.; Tomas, A.; Pardo, M. -P.; Guittard, M. *Phys. Status Solidi (a)* **1989**, *113*, K5−K7.
(19) Dabrowski, J.; Scheffler, M. *Phys. Rev. B* **1989**, *40*, 10391−10401.
(20) Chadi, D. J.; Chang, K. J. *Phys. Rev. Lett.* **1988**, *60*, 2187−2190.
(21) Lucazeau, G.; Leroy, J. *Spectrochim. Acta* **1978**, *34A*, 29−32.
(22) Liu, H. F.; Dolmanan, S. B.; Zhang, L.; Chua, S. J.; Chi, D. Z.; Heuken, M.; Tripathy, S. *J. Appl. Phys.* **2013**, *113*, 023510.
(23) Liu, H. F.; Chi, D. Z. *J. Vac. Sci. Technol. A* **2012**, *30*, 04D102.
(24) Chen, H. Crystal Growth and Optical Properties of Ga_2S_3. Master's Thesis, National Taiwan University of Science and Technology, Taiwan, 2013.
(25) Mushinskii, V. P.; Palaki, L. I.; Chebotaru, V. V. *Phys. Status Solidi (b)* **1977**, *83*, K149−K153.
(26) Aono, T.; Kase, K. *Solid State Commun.* **1992**, *81*, 303−305.
(27) Aono, T.; Kase, K. *Solid State Commun.* **1992**, *83*, 749−752.